Thin–Walled Structures 219 (2026) 114293

Contents lists available at ScienceDirect

Thin-Walled Structures

journal homepage: www.elsevier.com/locate/tws

Full length article

An isogeometric finite element implementation of visco-hyperelastic Kirchhoff–Love shells for large deformation and transient analysis

Seung-Hwan Boo [a], Hyomin Ryu [c], Seung Hwan Kim [b], Jaemin Kim [c,*]

[a] Division of Naval Architecture and Ocean Systems Engineering, Korea Maritime and Ocean University, Busan 49112, Republic of Korea
[b] Department of Neurosurgery, Sungkyunkwan University School of Medicine, Samsung Changwon Hospital, Changwon 51353, Republic of Korea
[c] Department of Mechanical Engineering, Changwon National University, Changwon 51140, Republic of Korea

ARTICLE INFO

Keywords:
Isogeometric
Kirchhoff–Love
Thin shell
Viscoelastic
Large deformation
Hyperelastic

ABSTRACT

This work presents an isogeometric finite element formulation for the large-deformation, time-dependent response of hyperelastic thin shells within the framework of the Kirchhoff–Love hypothesis. The out-of-plane stretch is statically condensed, such that the shell kinematics are fully described by the first and second fundamental forms of the mid-surface. The internal variable is considered to account for viscoelastic dissipation, and the backward Euler scheme is adopted for advancing the time evolution. The capability of the proposed formulation is demonstrated through two benchmark problems. For rubber balloon inflation, numerical results match the analytical solution, validating the formulation and implementation. For flat-shell inflation, parametric studies on the shear modulus and relaxation time reveal that viscoelastic relaxation can significantly alter load–deflection behavior and stress distributions under large strains. The present framework paves the way for employing three-dimensional constitutive equations for time-dependent, large-deformation analysis of thin shells within the isogeometric finite element analysis.

1. Introduction

Thin shell structures are widely encountered in engineering and biological systems, where they frequently undergo large, nonlinear, and time-dependent deformations. Examples include tires [1], airbags [2], thin films [3,4], air springs [5], pressure vessels [6], pneumatic actuators [7], and soft robotic grippers [8], as well as thin biological membranes such as those found in soft tissues [2,9–11]. The mechanical response of such structures is often dominated by both geometric and material nonlinearities, making their accurate modeling a challenging problem in computational mechanics.

For thin shells, the classical Kirchhoff–Love theory offers a simple yet robust kinematic description [12–14]. It assumes that lines initially normal to the mid-surface remain straight and normal after deformation, thereby neglecting transverse shear deformation [15,16]. This assumption leads to a pure bending–membrane formulation, where the mid-surface kinematics fully determine the shell configuration [17,18]. However, the weak form of the Kirchhoff–Love theory involves second derivatives of the displacement field and therefore requires basis functions with at least global C^1 continuity [13,19]. Since standard finite element analysis (FEA) based on Lagrange polynomials provides only C^0 continuity, the adoption of Kirchhoff–Love formulations has been limited. Instead, Reissner–Mindlin models, which require only C^0 continuity, have been more widely used for thick shells [20]. Nevertheless, such models suffer from shear-locking effects when applied to thin shells [15,21].

Isogeometric finite element analysis (IGA) [13] overcomes the long-standing limitations of standard finite element methods by employing basis functions commonly used in computer-aided design (CAD), most notably Non-Uniform Rational B-Splines (NURBS) [22,23]. These functions inherently provide the high-order continuity required for thin shell formulations, making IGA particularly well suited for Kirchhoff–Love shells. The ability to directly incorporate CAD geometries, exactly represent complex shapes, and construct globally C^1-conforming discretizations enables accurate and efficient shell modeling. Specifically, IGA can evaluate C^1-continuous geometrical quantities such as curvature directly, thus eliminating the need for specialized techniques [24–26] that are otherwise necessary in standard C^0 finite element approaches.

Since the introduction of the first geometrically nonlinear Kirchhoff–Love shell formulation in IGA [12], numerous extensions have been developed, including formulations for general hyperelastic materials [17] and elasto-plastic behavior [27]. A further advantage of the isogeometric approach lies in its computational efficiency. Due to the higher-order continuity of NURBS-based discretizations,

* Corresponding author.
E-mail address: jaeminkim@changwon.ac.kr (J. Kim).

https://doi.org/10.1016/j.tws.2025.114293
Received 8 September 2025; Received in revised form 30 October 2025; Accepted 21 November 2025
Available online 28 November 2025

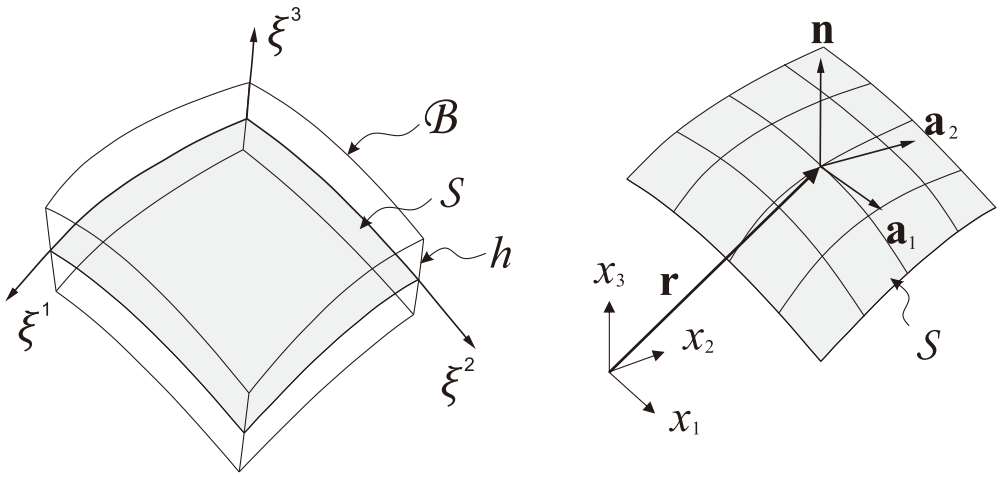

Fig. 1. Schematic representation of a Kirchhoff–Love shell in the current configuration: the continuum shell body $\mathcal{B}$, and its mid-surface $\mathcal{S}$. The curvilinear coordinates (ξ^1, ξ^2, ξ^3) represent the convective coordinate system, while (x_1, x_2, x_3) denote the Cartesian coordinates of a fixed spatial point. The covariant basis vectors of the mid-surface are $(\mathbf{a}_1, \mathbf{a}_2, \mathbf{a}_3 = \mathbf{n})$, where $\mathbf{n}$ is the unit normal to $\mathcal{S}$, and h denotes the current shell thickness.

fewer elements are required to achieve a given level of accuracy, which reduces the overall computational cost [28–31]. Moreover, the purely displacement-based nature of the Kirchhoff–Love formulation in IGA results in symmetric positive-definite system matrices, which are numerically stable and efficiently solvable [30,32,33]. In contrast, conventional formulations involving rotational degrees of freedom typically require mixed methods, leading to indefinite systems that are less stable and necessitate more sophisticated solvers [34–36].

Time-dependent and viscoelastic behaviors have been extensively studied in the context of shell and membrane models. Additive decomposition approaches have been applied to erythrocyte membranes [37], and three-dimensional viscoelastic formulations have been justified in [38]. Viscoelastic Reissner–Mindlin shell models have been developed in [39], while incompressible membrane models and quasi-linear viscoelastic formulations have been explored in [40,41]. From the perspective of surface elasticity [42,43], nonlinear surface viscoelasticity at finite strains has been formulated in [44], with coupled surface–bulk models applied to simulate cell–ECM interactions [45–47]. More recently, [48] developed an isogeometric implementation of the Kirchhoff–Love shell based on the Bezier extraction framework, focusing primarily on computational aspects. [41] analyzed large deformation and time-dependent responses of thin membrane shells using standard finite element analysis, though out-of-plane effects were neglected. The extended Kirchhoff–Love formulations of [49,50] incorporated out-of-plane normal stress components within hyperelastic models, while [17] presented general isogeometric Kirchhoff–Love shell formulations for compressible and incompressible hyperelastic materials. Furthermore, [21] proposed an isogeometric MITC shell formulation to alleviate shear and membrane locking within Reissner–Mindlin kinematics. Notably, although [26] introduced a finite element framework using mixed formulation for viscoelastic shells, a thermodynamically consistent time-dependent formulation of the Kirchhoff–Love shell within the isogeometric framework remains absent. Therefore, the present work addresses this gap by developing an isogeometric Kirchhoff–Love shell formulation for large deformation and time-dependent hyper-viscoelastic behavior with a thermodynamically consistent derivation.

In this study, we extend the isogeometric Kirchhoff–Love shell formulation to capture large-strain, time-dependent responses of incompressible hyper-viscoelastic materials within a thermodynamically consistent framework. The formulation accommodates arbitrary three-dimensional constitutive models for shell analysis, while the transverse normal strain is determined analytically from the plane stress condition along with the incompressibility constraint. This eliminates the need for additional degrees of freedom associated with thickness stretch, thereby preserving the purely surface-based kinematics of Kirchhoff–Love theory. To the best of our knowledge, this work presents the first nonlinear isogeometric Kirchhoff–Love shell formulation specifically developed for modeling the large-deformation and time-dependent behavior of hyper-viscoelastic materials.

The manuscript is organized as follows. In Section 2, we present a nonlinear shell theory, introducing key concepts from differential geometry, kinematics, and the general form of constitutive equations and stress resultants. In Section 3, we specialize the strain energy and dissipation potentials for a visco-hyperelastic Kirchhoff–Love shell model. Section 4 describes the isogeometric finite element implementation, including the NURBS-based surface representation, the weak form derivation, and the numerical solution procedure. Section 5 provides numerical simulations for two benchmark problems: (i) the inflation of a rubber balloon, used to validate the implementation against an analytical solution, and (ii) the inflation of a flat shell, demonstrating the model's ability to capture large deformation and time-dependent responses. Finally, Section 6 concludes the study and outlines potential directions for future research.

2. A nonlinear shell theory

2.1. Geometry

Let $\mathcal{B}_0$ and $\mathcal{B}$ represent the reference and current configurations of a continuum body, respectively. Hereafter, quantities with a subscript 0 denote the reference configuration, while those without the subscript refer to the current configuration. The mid-surface and thickness of $\mathcal{B}_0$ and $\mathcal{B}$ are denoted as $(\mathcal{S}_0, h_0)$ and $(\mathcal{S}, h)$, respectively (see Fig. 1).

$$\mathbf{X}(\xi^1, \xi^2, \xi^3) = \mathbf{R}(\xi^1, \xi^2) + \xi^3 \mathbf{N}(\xi^1, \xi^2) \quad \text{on} \quad \mathcal{S}_0 \tag{1}$$

$$\mathbf{x}(\xi^1, \xi^2, \xi^3, t) = \mathbf{r}(\xi^1, \xi^2, t) + \xi^3 \mathbf{d}(\xi^1, \xi^2, t) \quad \text{on} \quad \mathcal{S} \tag{2}$$

Here, $\mathbf{R}$ and $\mathbf{r}$ are the position vectors on the mid-surfaces $\mathcal{S}_0$ and $\mathcal{S}$, respectively. The thickness stretch of the membrane is given by $\lambda_3 = h/h_0$, and we introduce $\mathbf{d} = \lambda_3 \mathbf{n}$, which combines the thickness stretch and outward normal vectors.

Two sets of reference basis vectors ($\mathbf{A}_\alpha$ and $\mathbf{A}^\alpha$) are associated with the curvilinear coordinates ξ^α on $\mathcal{S}_0$, while the current basis vectors ($\mathbf{a}_\alpha$ and $\mathbf{a}^\alpha$) are defined on $\mathcal{S}$:

$$\mathbf{A}_\alpha = \frac{\partial \mathbf{R}}{\partial \xi^\alpha}, \quad \mathbf{A}^\alpha = \frac{\partial \xi^\alpha}{\partial \mathbf{R}} \quad \text{and} \quad \mathbf{N} \equiv \mathbf{A}^3 = \frac{\mathbf{A}_1 \times \mathbf{A}_2}{|\mathbf{A}_1 \times \mathbf{A}_2|} = \mathbf{A}_3 \tag{3}$$

$$\mathbf{a}_\alpha = \frac{\partial \mathbf{r}}{\partial \xi^\alpha}, \quad \mathbf{a}^\alpha = \frac{\partial \xi^\alpha}{\partial \mathbf{r}} \quad \text{and} \quad \mathbf{n} \equiv \mathbf{a}^3 = \frac{\mathbf{a}_1 \times \mathbf{a}_2}{|\mathbf{a}_1 \times \mathbf{a}_2|} = \mathbf{a}_3 \tag{4}$$

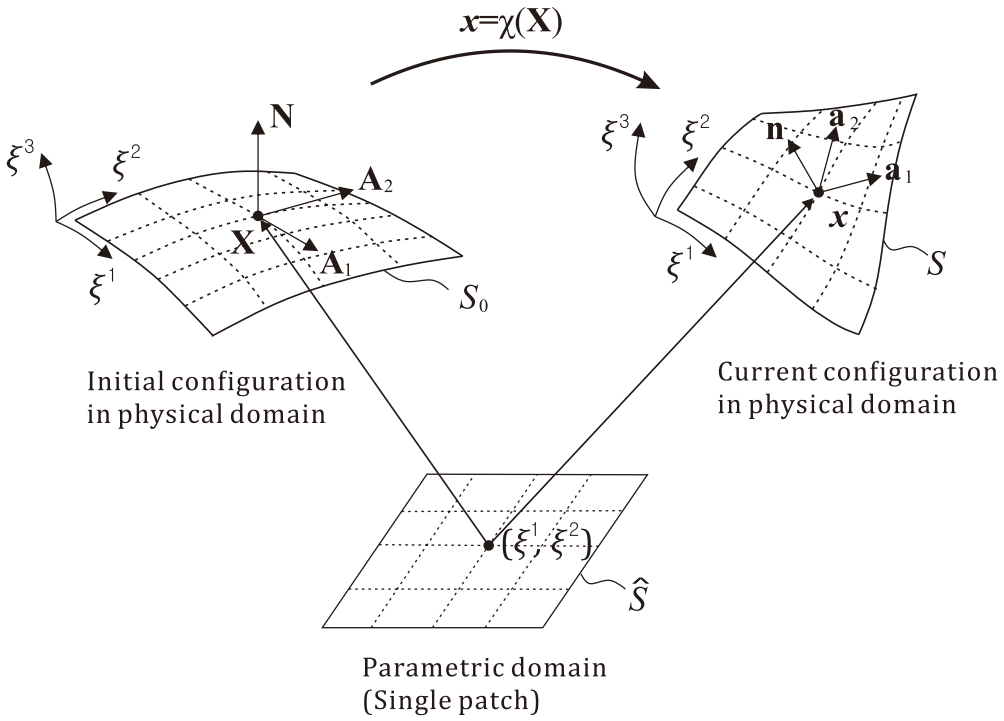

Fig. 2. Illustration of the isogeometric analysis (IGA) mapping concept for a single NURBS patch. The shell mid-surface is represented in three spaces: (i) the parametric domain $\hat{\mathcal{S}}$, (ii) the initial configuration $\mathcal{S}_0$, and (iii) the current configuration $\mathcal{S}$ in the physical domain. The geometric mapping from $\hat{\mathcal{S}}$ to $\mathcal{S}_0$ is defined by the NURBS surface representation using control points, basis functions, and knot vectors. The motion of the shell is described by the mapping $\mathbf{x} = \chi(\mathbf{X})$ from $\mathcal{S}_0$ to $\mathcal{S}$.

Here, $\mathbf{A}_\alpha$ and $\mathbf{A}^\beta$ are the covariant and contravariant basis vectors in the reference configuration, while $\mathbf{a}_\alpha$ and $\mathbf{a}^\beta$ are their counterparts in the current configuration. Note that $\mathbf{N}$ and $\mathbf{n}$ are the outward normal vectors. These basis vectors satisfy the orthogonality conditions $\mathbf{A}^i \cdot \mathbf{A}_j = \delta^i_j$ and $\mathbf{a}^i \cdot \mathbf{a}_j = \delta^i_j$, where δ^i_j is the Kronecker delta, with $\delta^i_j = 1$ for $i = j$ and $\delta^i_j = 0$ otherwise. Although covariant and contravariant basis vectors are not necessarily orthogonal, they remain linearly independent, satisfying $(\mathbf{a}_1 \times \mathbf{a}_2) \cdot \mathbf{a}_3 \neq 0$ to ensure they do not lie in a plane.

The covariant basis vectors are related to the contravariant basis vectors through the covariant metric tensors (A_{ij}, a_{ij}), with their components given by:

$$\mathbf{A}_i = A_{ij}\mathbf{A}^j \quad \text{with} \quad A_{ij} = A_{ji} = \mathbf{A}_i \cdot \mathbf{A}_j \tag{5}$$

$$\mathbf{a}_i = a_{ij}\mathbf{a}^j \quad \text{with} \quad a_{ij} = a_{ji} = \mathbf{a}_i \cdot \mathbf{a}_j \tag{6}$$

The curvature tensors on the mid-surfaces $\mathcal{S}_0$ and $\mathcal{S}$ are defined as [51]:

$$B_{\alpha\beta} = \mathbf{A}_{\alpha,\beta} \cdot \mathbf{N} = -\mathbf{A}_\alpha \cdot \mathbf{N}_{,\beta} \tag{7}$$

$$b_{\alpha\beta} = \mathbf{a}_{\alpha,\beta} \cdot \mathbf{d} = -\mathbf{a}_\alpha \cdot \mathbf{d}_{,\beta} \tag{8}$$

where $(\bullet)_{,\beta}$ denotes partial differentiation with respect to ξ^β.

The covariant basis vectors in the three-dimensional shell-space are expressed as:

$$\mathbf{G}_\alpha = \mathbf{X}_{,\alpha} = \mathbf{A}_\alpha + \xi^3\mathbf{N}_{,\alpha}, \quad \mathbf{G}_3 = \frac{\partial \mathbf{X}}{\partial \xi^3} = \mathbf{N} \tag{9}$$

$$\mathbf{g}_\alpha = \mathbf{x}_{,\alpha} = \mathbf{a}_\alpha + \xi^3\mathbf{d}_{,\alpha}, \quad \mathbf{g}_3 = \frac{\partial \mathbf{x}}{\partial \xi^3} = \mathbf{d} \tag{10}$$

Here, $\mathbf{G}_i$ and $\mathbf{g}_i$ denote the covariant basis vectors at an elevation ξ^3 from the mid-surface in the reference and current configurations, respectively. The components of the covariant and contravariant metric tensors in the shell-space are:

$$G_{ij} = \mathbf{G}_i \cdot \mathbf{G}_j \quad \text{and} \quad G^{ij} = \mathbf{G}^i \cdot \mathbf{G}^j \tag{11}$$

$$g_{ij} = \mathbf{g}_i \cdot \mathbf{g}_j \quad \text{and} \quad g^{ij} = \mathbf{g}^i \cdot \mathbf{g}^j \tag{12}$$

where $\mathbf{G}^i$ and $\mathbf{g}^i$ are the contravariant basis vectors in the reference and current configurations, satisfying $\mathbf{G}^i \cdot \mathbf{G}_j = \delta^i_j$, $\mathbf{g}^i \cdot \mathbf{g}_j = \delta^i_j$.

2.2. Kinematics

The three-dimensional deformation gradient in shell-space is then defined as

$$\mathbf{F} = \nabla\chi = \mathbf{g}_i \otimes \mathbf{G}^i \tag{13}$$

The corresponding right Cauchy–Green deformation tensor is given by

$$\mathbf{C} = \mathbf{F}^{\mathrm{T}} \cdot \mathbf{F} = g_{ij}\mathbf{G}^i \otimes \mathbf{G}^j \tag{14}$$

Substituting Eqs. (10) and (12) into Eq. (14), the right Cauchy–Green deformation tensor expands as

$$\begin{aligned}\mathbf{C} = {} & g_{\alpha\beta}\mathbf{G}^\alpha \otimes \mathbf{G}^\beta + \lambda_3^2\mathbf{G}^3 \otimes \mathbf{G}^3 + \left[\mathbf{a}_\alpha \cdot \mathbf{d} + \xi^3\mathbf{d}_{,\alpha} \cdot \mathbf{d}\right]\mathbf{G}^\alpha \otimes \mathbf{G}^3 \\ & + \left[\mathbf{a}_\beta \cdot \mathbf{d} + \xi^3\mathbf{d}_{,\beta} \cdot \mathbf{d}\right]\mathbf{G}^3 \otimes \mathbf{G}^\beta\end{aligned} \tag{15}$$

where the term $\mathbf{a}_\alpha \cdot \mathbf{d} = 0$ since $\mathbf{a}_\alpha$ is always orthogonal to $\mathbf{n}$. The term $\xi^3\mathbf{d}_{,\alpha} \cdot \mathbf{d}$ is negligible as the thickness stretch variation is minimal for a thin shell. Thus, the right Cauchy–Green deformation tensor simplifies to

$$\mathbf{C} \approx g_{\alpha\beta}\mathbf{G}^\alpha \otimes \mathbf{G}^\beta + \lambda_3^2\mathbf{G}^3 \otimes \mathbf{G}^3 \tag{16}$$

Similarly, by neglecting thickness stretch differentiation, the covariant and contravariant metric tensors reduce to

$$G_{\alpha\beta} \approx A_{\alpha\beta} - 2\xi^3 B_{\alpha\beta} \tag{17}$$

$$g_{\alpha\beta} \approx a_{\alpha\beta} - 2\xi^3 b_{\alpha\beta} \tag{18}$$

The Green–Lagrange strain tensor is then expressed as

$$\mathbf{E} = \frac{1}{2}(\mathbf{C} - \mathbf{I}) = \left(\varepsilon_{\alpha\beta} + \kappa_{\alpha\beta}\xi^3\right)\mathbf{G}^\alpha \otimes \mathbf{G}^\beta + \frac{1}{2}\left(\lambda_3^2 - 1\right)\mathbf{G}^3 \otimes \mathbf{G}^3 \tag{19}$$

where the mid-surface strain and curvature tensors were defined as

$$\varepsilon_{\alpha\beta} = \frac{1}{2}\left(a_{\alpha\beta} - A_{\alpha\beta}\right) \tag{20}$$

$$\kappa_{\alpha\beta} = -b_{\alpha\beta} + B_{\alpha\beta} \tag{21}$$

corresponding to stretching and bending strains, respectively. The identity tensor on the referential mid-surface is given by $\mathbf{I} = G_{\alpha\beta}\mathbf{G}^{\alpha} \otimes \mathbf{G}^{\beta} + \mathbf{G}^{3} \otimes \mathbf{G}^{3}$. The components of the right Cauchy–Green deformation and Green–Lagrange strain tensors are denoted as C_{ij} and E_{ij}, respectively. The in-plane strains on the mid-surface of shell continuum can be expressed by

$$E_{\alpha\beta} = \varepsilon_{\alpha\beta} + \xi^{3}\kappa_{\alpha\beta} \tag{22}$$

where the transverse shear strains vanish ($E_{\alpha 3} = 0$), while the transverse normal strain does not ($E_{33} \neq 0$). Note that E_{33} represents the thickness deformation, which is determined analytically by enforcing the plane-stress condition and the incompressibility constraint ($J = 1$). The plane-stress condition implies that the out-of-plane component of the first Piola–Kirchhoff stress tensor vanishes ($P^{33} = 0$). The hydrostatic pressure p is subsequently derived from these two constraints in Section 3.2

For later use, the deformation gradient $\mathbf{F}$ is decomposed multiplicatively into volumetric and isochoric parts:

$$\mathbf{F} = \mathbf{F}_{v} \cdot \overline{\mathbf{F}}, \quad \text{where} \quad \mathbf{F}_{v} = J^{1/3}\mathbf{I}, \quad \overline{\mathbf{F}} = J^{-1/3}\mathbf{F} \tag{23}$$

where $\mathbf{F}_{v}$ is the volumetric part and $\overline{\mathbf{F}}$ is the isochoric part of $\mathbf{F}$. This leads to the multiplicative decomposition of the right Cauchy–Green tensor:

$$\mathbf{C} = \mathbf{C}_{v} \cdot \overline{\mathbf{C}}, \quad \text{where} \quad \mathbf{C}_{v} = J^{2/3}\mathbf{I}, \quad \overline{\mathbf{C}} = \overline{\mathbf{F}}^{\mathrm{T}} \cdot \overline{\mathbf{F}} \tag{24}$$

where $\mathbf{C}_{v}$ and $\overline{\mathbf{C}}$ represent the volumetric and isochoric components of $\mathbf{C}$, respectively. Note that the trace and determinant of $\mathbf{C}$ are obtained by

$$\operatorname{tr}\mathbf{C} = g_{\alpha\beta}G^{\alpha\beta} + \lambda_{3}^{2}G^{33} \tag{25}$$

$$\det\mathbf{C} = \frac{|g_{\alpha\beta}|\lambda_{3}^{2}}{|G_{\alpha\beta}|} = J_{0}^{2}\lambda_{3}^{2} \tag{26}$$

where J_0 is the in-plane Jacobian determinant, which is related to the Jacobian determinant $J = \det(\mathbf{F})$ by

$$J = J_{0}\lambda_{3} \tag{27}$$

The invariants of the deformation tensor and their relation to the principal stretches are given by

$$I_{1} = \operatorname{tr}\mathbf{C} = \lambda_{1}^{2} + \lambda_{2}^{2} + \lambda_{3}^{2} \tag{28}$$

$$\overline{I}_{1} = \operatorname{tr}\overline{\mathbf{C}} = J^{-2/3}I_{1} \tag{29}$$

Note that $\lambda_3 = \sqrt{C_{33}}$ is the thickness stretch in Kirchhoff–Love shell model. Lastly, we introduce an internal (or state) variable.

$$\boldsymbol{\mathcal{A}} \quad \text{with} \quad \mathcal{A}_{ij} = \mathcal{A}_{ji} \quad \forall i, j \tag{30}$$

where $\boldsymbol{\mathcal{A}}$ is a second-order symmetric structural tensor that quantifies the relaxation viscoelastic contribution.

2.3. Constitutive relations

We consider the strain energy density Ψ, assuming that it depends on the deformation and on viscous dissipation processes [52]:

$$\Psi(\mathbf{u}, \boldsymbol{\mathcal{A}}) \tag{31}$$

where $\boldsymbol{\mathcal{A}}$ denotes the internal variable (a second-order tensor) introduced to capture the dissipation associated with viscoelastic deformation. For a system containing a viscoelastic network, the rate of change of the total strain energy $\mathcal{G}$ must account for several effects [46,52,53], and can be expressed as

$$\dot{\mathcal{G}} = \int_{V} \dot{\Psi}\,\mathrm{d}V - \int_{V} \mathbf{B}\cdot\dot{\boldsymbol{x}}\,\mathrm{d}V - \int_{S} \mathbf{T}\cdot\dot{\boldsymbol{x}}\,\mathrm{d}S \tag{32}$$

where the second and third terms represent the rates of mechanical work by the body force $\mathbf{B}$ and the traction vector $\mathbf{T}$, respectively. The overdot denotes a material time derivative.

In the following, we adopt the second Piola–Kirchhoff stress tensor $\mathbf{S} = S^{ij}\mathbf{G}_{i} \otimes \mathbf{G}_{j}$, related to the first Piola–Kirchhoff stress tensor $\mathbf{P}$ by $\mathbf{S} = \mathbf{F}^{-1}\mathbf{P}$ via a pull-back operation. While $\mathbf{S}$ lacks a direct physical interpretation in terms of surface tractions, it is symmetric and parameterized with respect to the material coordinates, which is advantageous for finite element implementation [52]. Rewriting Eq. (32) in terms of stresses and strains [2,12,17], we have

$$\dot{\mathcal{G}} = \int_{V} \dot{\Psi}\,\mathrm{d}V - \int_{V} \mathbf{S} : \dot{\mathbf{E}}\,\mathrm{d}V \leq 0 \tag{33}$$

where the symbol $\{:\}$ denotes the double contraction.

Applying the chain rule, the rate of change of the strain energy density is

$$\dot{\Psi} = \frac{\partial\Psi}{\partial\mathbf{E}} : \dot{\mathbf{E}} + \frac{\partial\Psi}{\partial\boldsymbol{\mathcal{A}}} : \dot{\boldsymbol{\mathcal{A}}} \tag{34}$$

Substituting Eq. (34) into Eq. (33) and rearranging terms, we obtain

$$\dot{\mathcal{G}} = \int_{V} \left(\frac{\partial\Psi}{\partial\mathbf{E}} - \mathbf{S}\right) : \dot{\mathbf{E}}\,\mathrm{d}V + \int_{V} \frac{\partial\Psi}{\partial\boldsymbol{\mathcal{A}}} : \dot{\boldsymbol{\mathcal{A}}}\,\mathrm{d}V \leq 0 \tag{35}$$

From thermodynamic considerations, the strain energy of the system cannot increase, i.e., $\dot{\mathcal{G}} \leq 0$. Each integral in Eq. (35) corresponds to a distinct dissipation mechanism: the first term is associated with mechanical equilibrium, while the second accounts for non-equilibrium processes such as viscous deformation. The inequality must hold pointwise in space and time.

According to the Coleman–Noll procedure [52], each integrand in Eq. (35) must therefore be non-positive. Following the seminal works of Coleman and Noll [52,54], the thermodynamically consistent constitutive relations can be expressed as

$$\mathbf{S} = \frac{\partial\Psi(\mathbf{u}, \boldsymbol{\mathcal{A}})}{\partial\mathbf{E}} = 2\frac{\partial\Psi(\mathbf{u}, \boldsymbol{\mathcal{A}})}{\partial\mathbf{C}}, \quad \frac{\partial\Psi(\mathbf{u}, \boldsymbol{\mathcal{A}})}{\partial\boldsymbol{\mathcal{A}}} : \dot{\boldsymbol{\mathcal{A}}} \leq 0 \tag{36}$$

where the first relation defines the second Piola–Kirchhoff stress tensor in terms of the strain energy potential, and the second relation represents the dissipation inequality associated with the evolution of the internal variable $\boldsymbol{\mathcal{A}}$.

2.4. Stress resultants

The Kirchhoff–Love shell formulation considers a three-dimensional solid as a two-dimensional midsurface with an associated thickness. Accordingly, the internal forces are obtained as stress resultants through-thickness integration of the Piola–Kirchhoff stress components. These stress resultants decompose into the membrane force $n_{\alpha\beta}$ and the bending moment $m_{\alpha\beta}$, expressed as

$$n^{\alpha\beta} = \int_{-h_0/2}^{h_0/2} S^{\alpha\beta}J_{0}\,\mathrm{d}\xi^{3} \quad \text{and} \quad m^{\alpha\beta} = \int_{-h_0/2}^{h_0/2} S^{\alpha\beta}J_{0}\xi^{3}\,\mathrm{d}\xi^{3} \tag{37}$$

where $n_{\alpha\beta}$ and $m_{\alpha\beta}$ denote the membrane forces and bending moments, respectively. This stress-resultant approach is particularly suitable for isogeometric Kirchhoff–Love shells, since the C^1-continuity of spline basis functions naturally ensures accuracy for bending-dominated problems [17,21,27].

3. Specific models

3.1. Strain energy density

The total strain energy is additively decomposed into equilibrium and non-equilibrium parts, written as

$$\Psi(\mathbf{u}, \boldsymbol{\mathcal{A}}) = \Psi_{eq}(\mathbf{u}) + \Psi_{neq}(\mathbf{u}, \boldsymbol{\mathcal{A}}) \tag{38}$$

where Ψ_{eq} and Ψ_{neq} represent the equilibrium and non-equilibrium contributions, respectively.

For the equilibrium term Ψ_{eq}, we adopt a neo-Hookean hyperelastic model to describe the elastic response [46,52]:

$$\Psi_{eq} = \Psi_{el} + p_h\,(J-1), \quad \Psi_{el} = \frac{\mu_e}{2}\left(I_1 - 3\right) \tag{39}$$

where Ψ_{el} is the purely elastic energy, μ_e is the equilibrium shear modulus, and p_h is a Lagrange multiplier enforcing incompressibility, which can be identified with the hydrostatic pressure [52].

For the non-equilibrium contribution Ψ_{neq}, we adopt a finite viscoelastic model [55], which enables the formulation to capture the time-dependent viscoelastic behavior of the material:

$$\Psi_{neq} = \frac{\mu_v}{2}\left[\boldsymbol{\mathcal{A}} : \overline{\mathbf{C}} - 3 - \ln(\det \boldsymbol{\mathcal{A}})\right] \tag{40}$$

Here μ_v represents the non-equilibrium shear modulus. It is important to note that the non-equilibrium strain energy density Ψ_{neq} depends on the isochoric right Cauchy–Green deformation tensor $\overline{\mathbf{C}}$ and the internal variables $\boldsymbol{\mathcal{A}}$. The isochoric part of the deformation thus governs the time-dependent relaxation behavior, while the volumetric response remains purely elastic [55].

3.2. Hydrostatic pressure

By substituting Eqs. (38) and (39) into Eq. (36), the stress tensor $\mathbf{S}$ can be expressed as

$$\mathbf{S} = \hat{\mathbf{S}} - p_h \mathbf{C}^{-1} \quad \text{with} \quad \hat{\mathbf{S}} = 2\left(\frac{\partial \Psi_{el}}{\partial \mathbf{C}} + \frac{\partial \Psi_{neq}}{\partial \mathbf{C}}\right) \tag{41}$$

where the derivatives of the strain energy functions are given by

$$\frac{\partial \Psi_{el}}{\partial \mathbf{C}} = \frac{\mu_e}{2}\mathbf{I}, \quad \frac{\partial \Psi_{neq}}{\partial \mathbf{C}} = \frac{\mu_v}{2} J^{-2/3} \boldsymbol{\mathcal{A}} \tag{42}$$

The plane-stress condition, $S^{33} = 0$, yields the following expression for the hydrostatic pressure p_h:

$$S^{33} = \mu_e + \mu_v J^{-2/3} \mathcal{A}_{33} - p_h C^{33} = 0 \Rightarrow p_h = \lambda_3^2\left(\mu_e + \mu_v J^{-2/3} \mathcal{A}_{33}\right) \tag{43}$$

where the relations $C^{33}C_{33} = 1$ and $\mathcal{A}^{33}\mathcal{A}_{33} = 1$ have been used. Here, λ_3 denotes the thickness stretch, and $\lambda_i = \sqrt{C_{ii}}$. The incompressibility condition $\lambda_1\lambda_2\lambda_3 = 1$ indicates that the in-plane stretches λ_1 and λ_2 of the shell mid-surface uniquely determine the thickness stretch λ_3.

3.3. Evolution equation

The visco-relaxation internal variables $\boldsymbol{\mathcal{A}}$ evolve according to [55]:

$$\dot{\boldsymbol{\mathcal{A}}} = \frac{1}{\tau}\left(\overline{\mathbf{C}}^{-1} - \boldsymbol{\mathcal{A}}\right) \tag{44}$$

where the superposed dot denotes the material time derivative, and τ is the relaxation time. When $\mathbf{C}^{-1} = \boldsymbol{\mathcal{A}}$, the system reaches equilibrium, indicating complete stress relaxation. Importantly, this evolution law inherently satisfies the dissipation inequality [55,56]. For time integration, we employ a backward Euler discretization of Eq. (44), leading to the following update rule for the internal variable $\boldsymbol{\mathcal{A}}$:

$$\boldsymbol{\mathcal{A}}_{t+\Delta t} = \left(1 + \frac{\Delta t}{\tau}\right)^{-1}\left(\boldsymbol{\mathcal{A}}_t + \frac{\Delta t}{\tau}\,\overline{\mathbf{C}}^{-1}\right) \tag{45}$$

where the subscripts $t + \Delta t$ and t refer to the current and previous time steps, respectively.

4. Isogeometric finite element analysis

This section presents the isogeometric finite element formulation, implemented in FEniCS and based on the nonlinear theory described in Sections 2 and 3 [57,58]. For isogeometric discretization, we employ tIGAr library [59], which provides a direct interface between NURBS-based geometry and standard finite element solvers. The procedure begins with the NURBS surface representation and the strong form of the governing equations, followed by derivation of the weak form and discretization. Here, we specifically investigate the time-dependent viscoelastic response under large deformations, neglecting external forces, i.e., $\mathbf{B} = 0$ and $\mathbf{T} = 0$.

4.1. NURBS surface

Non-Uniform Rational B-Splines (NURBS) are a standard tool for modeling curves and surfaces in computer-aided design (CAD) systems [22,23,60]. B-Splines are piecewise polynomial curves defined as linear combinations of B-Spline basis functions. A knot vector Ξ is a non-decreasing sequence of real numbers that parameterizes the B-Spline space:

$$\Xi = \{\xi_1, \xi_2, \ldots, \xi_{n+p+1}\} \tag{46}$$

where p denotes the polynomial degree of the basis functions and n is the number of basis functions (also equal to the number of control points). Given a knot vector Ξ, the B-Spline basis functions are defined recursively:

$$\overline{N}_{i,p}(\xi) = \begin{cases} 1 & \text{if } \xi_i < \xi < \xi_{i+1} \\ 0 & \text{otherwise} \end{cases} \tag{47}$$

$$\overline{N}_{i,p}(\xi) = \frac{\xi - \xi_i}{\xi_{i+p} - \xi_i} N_{i,p-1}(\xi) + \frac{\xi_{i+p+1} - \xi}{\xi_{i+p+1} - \xi_{i+1}} N_{i+1,p-1}(\xi) \tag{48}$$

where $\overline{N}_{i,p}(\xi)$ is the B-Spline basis functions of degree p for $i = 1, 2, \ldots, n$ (see Fig. 3).

A 3D NURBS surface $S(\xi^1, \xi^2)$, parameterized by the curvilinear coordinates (ξ^1, ξ^2), is employed to model the shell mid-surface. We denote the physical domain (i.e., the 3D shell mid-surface) by $\mathcal{S}$, and the parametric domain by $\hat{\mathcal{S}}$, where the latter is a two-dimensional rectangle (see Fig. 2). The geometrical mapping $\mathbf{x} : \hat{\mathcal{S}} \subset \mathbb{R}^2 \to \mathcal{S} \subset \mathbb{R}^3$ takes material points from the parametric domain and maps them to the corresponding points in the physical domain.

Given the knot vectors $\Xi_1 = \{\xi_1^1, \ldots, \xi_{n+p+1}^1\}$ and $\Xi_2 = \{\xi_1^2, \ldots, \xi_{m+q+1}^2\}$, the shell mid-surface is constructed using a tensor-product approach [13,22]:

$$S(\xi^1, \xi^2) = \sum_{i=1}^{n}\sum_{j=1}^{m} \overline{N}_{i,p}(\xi^1)\,\overline{N}_{j,q}(\xi^2)\,\widetilde{\mathbf{x}}_{ij} \tag{49}$$

where $\overline{N}_{i,p}(\xi^1)$ and $\overline{N}_{j,q}(\xi^2)$ are B-Spline basis functions of degree p and q in the ξ^1 and ξ^2 directions, respectively, and $\widetilde{\mathbf{x}}_{ij}$ are the 3D control points.

The set of control points $\widetilde{\mathbf{x}}_{ij}$ defines the control mesh, while the domain $[\xi_1^1, \xi_{n+p+1}^1] \times [\xi_1^2, \xi_{m+q+1}^2]$ is referred to as a patch, with each non-zero knot span defining an element [13]. Since the control points do not generally lie on the mid-surface of the shell, the superimposed tilde ($\widetilde{\cdot}$) is used to distinguish quantities defined on the control mesh from those associated with the physical shell mid-surface (see Fig. 4).

Using standard finite element notation, a single index A can be introduced to map the tensor-product indices (i, j):

$$S(\xi^1, \xi^2) = \sum_{A=1}^{n_{cp}} \overline{N}_A(\xi^1, \xi^2)\,\widetilde{\mathbf{x}}_A, \quad (n_{cp} = n \times m) \tag{50}$$

where $\overline{N}_A(\xi^1, \xi^2) = \overline{N}_{i,p}(\xi^1)\,\overline{N}_{j,q}(\xi^2)$ denotes the B-Spline shape function associated with control point A, and n_{cp} is the total number of control points.

A NURBS surface is obtained by introducing a weight w_A for each control point $\widetilde{\mathbf{x}}_A$:

$$S(\xi^1, \xi^2) = \frac{\sum_{A=1}^{n_{cp}} \overline{N}_A(\xi^1, \xi^2)\, w_A\, \widetilde{\mathbf{x}}_A}{\sum_{A=1}^{n_{cp}} \overline{N}_A(\xi^1, \xi^2)\, w_A} = \sum_{A=1}^{n_{cp}} N_A(\xi^1, \xi^2)\,\widetilde{\mathbf{x}}_A \tag{51}$$

where $N_A(\xi^1, \xi^2)$ are the NURBS basis functions. The weights w_A are prescribed by the CAD geometry and are not treated as variables in the finite element analysis.

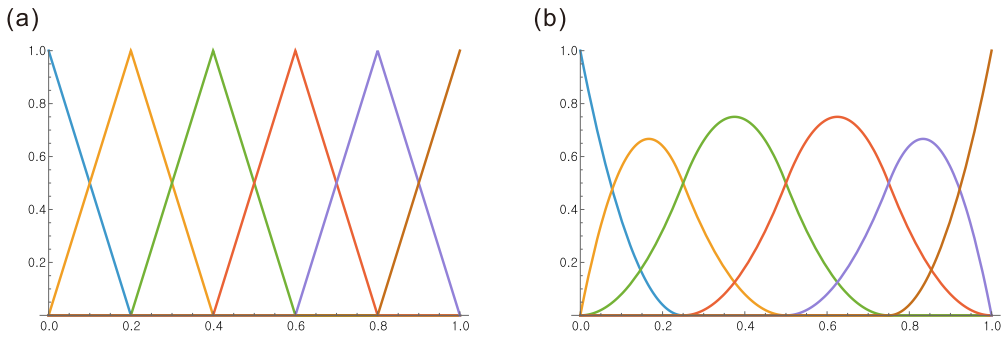

Fig. 3. B-Spline basis functions for polynomial degrees $p = 1$ and $p = 2$ with $n = 6$ control points, constructed using the open knot vector $\Xi = [0, 0, 0.2, 0.4, 0.6, 0.8, 1.0, 1.0]$. (a) For $p = 1$, the basis functions are piecewise linear with C^0 continuity at internal knots, corresponding to standard piecewise linear finite element shape functions, whereas (b) for $p = 2$, they are quadratic with C^1 continuity at internal knots, corresponding to the basis functions used in isogeometric finite element analysis (IGA).

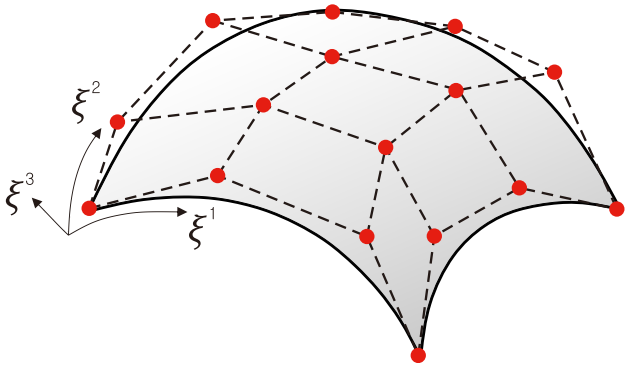

Fig. 4. NURBS surface representation with curvilinear coordinates (ξ^1, ξ^2, ξ^3). The red dots denote the control points, the black dashed lines form the control mesh, and the gray surface represents the resulting NURBS surface constructed from the control points, basis functions, and knot vectors.

Remark 1 (*Relationship Between NURBS and B-Splines*)**.** When all weights are equal, NURBS surfaces reduce to their B-Spline counterparts. This follows directly from the partition of unity property and the definition of NURBS basis functions [22]. In this work, we denote the basis functions by $N_A(\xi^1, \xi^2)$, irrespective of whether they are rational (NURBS) or non-rational (B-Splines). Hence, the term "NURBS" is used in a generalized sense to also encompass B-Spline formulations.

4.2. Weak form

The weak form of the problem is obtained by introducing a set of test functions that satisfy the necessary integrability conditions [14]. Applying the principle of virtual work yields the governing equations for the nonlinear thin shell (Kirchhoff–Love shell) theory, which can be written as

$$\delta\mathcal{W}(\mathbf{u}, \delta\mathbf{u}) = \delta\mathcal{W}_{int} - \delta\mathcal{W}_{ext} = 0 \quad \forall\, \delta\mathbf{u} \in \mathcal{V} \tag{52}$$

where the quasi-static internal and external virtual work are defined as

$$\delta\mathcal{W}_{int} = \int_{S_0} \left(\overline{\mathbf{n}} : \delta\boldsymbol{\varepsilon} + \overline{\mathbf{m}} : \delta\boldsymbol{\kappa}\right) \mathrm{d}S_0 \tag{53}$$

$$\delta\mathcal{W}_{ext} = \int_{S_0} \overline{\mathbf{f}} \cdot \delta\mathbf{u}\, \mathrm{d}S_0 \tag{54}$$

with $\overline{\mathbf{f}}$ denoting the external load on the shell mid-surface, $\delta\mathbf{u}$ the virtual displacement, and $\delta\boldsymbol{\varepsilon}$ and $\delta\boldsymbol{\kappa}$ the corresponding virtual membrane strain and change in curvature, respectively. Here, S_0 represents the shell mid-surface in the reference (undeformed) configuration, and $\mathrm{d}S_0 = \sqrt{|A_{\alpha\beta}|}\, \mathrm{d}\xi^1\, \mathrm{d}\xi^2$ is the associated surface element. It is important to note that this formulation assumes the differential volume element can be approximated by $\mathrm{d}V_0 \approx h_0\, \mathrm{d}S_0$, an approximation valid for thin shells.

The weak form can be stated as follows: find the trial function $\mathbf{u} \in \mathcal{S}$ such that Eq. (52) holds for all admissible test functions $\delta\mathbf{u} \in \mathcal{V}$. The sets of admissible trial (solution) and test (variation) functions are defined as

$$\mathcal{S} = \{\mathbf{u} \,|\, \mathbf{u} \in H^2,\ \mathbf{u} = \check{\mathbf{u}} \text{ on } \Gamma_u\}, \tag{55}$$

$$\mathcal{V} = \{\delta\mathbf{u} \,|\, \delta\mathbf{u} \in H^2,\ \delta\mathbf{u} = 0 \text{ on } \Gamma_u\}, \tag{56}$$

where $\check{\mathbf{u}}$ denotes the prescribed displacement values on the Dirichlet boundary Γ_u, and H^2 is the Sobolev space of order two. The use of H^2 is necessary to guarantee that both the first and second derivatives of the displacement field are square-integrable. This requirement arises from the Kirchhoff–Love shell formulation, which demands C^1-continuity of the displacement field.

4.3. Finite element formulation

The displacement field of the Kirchhoff–Love shell is interpolated using NURBS basis functions in Voigt notation as [13,61]:

$$\mathbf{u} = \sum_{A=1}^{n_{cp}} N_A\, \mathbf{u}_A, \tag{57}$$

where N_A denotes the NURBS basis function defined on the physical domain, n_{cp} is the number of control points, and $\mathbf{u}_A$ is the displacement vector associated with the Ath control point. Each vector $\mathbf{u}_A$ contains three Cartesian components u^i_A, resulting in a total of $3n_{cp}$ degrees of freedom. The global degree-of-freedom index is defined as $r = 3(A-1) + i \in [1, 3n_{cp}]$, such that $u_r = u^i_A$.

The derivative of $\mathbf{u}$ with respect to the rth degree of freedom is given by [2,16,17,62]:

$$\delta_r\mathbf{u} = \frac{\partial\mathbf{u}}{\partial u_r} = N_A\mathbf{e}_i, \tag{58}$$

where $\mathbf{e}_i$ $(i = 1, 2, 3)$ are the orthonormal basis vectors. Similarly, the derivatives of the strain components $\varepsilon_{\alpha\beta}$ and $\kappa_{\alpha\beta}$ with respect to u_r are expressed as [2,17]:

$$\delta_r\varepsilon_{\alpha\beta} = \tfrac{1}{2}\left(\delta_r\mathbf{a}_\alpha \cdot \mathbf{a}_\beta + \mathbf{a}_\alpha \cdot \delta_r\mathbf{a}_\beta\right), \tag{59}$$

$$\delta_r\kappa_{\alpha\beta} = -\lambda_3\left(\delta_r\mathbf{a}_{\alpha,\beta} \cdot \mathbf{a}_3 + \mathbf{a}_{\alpha,\beta} \cdot \delta_r\mathbf{a}_3\right) - \delta_r\lambda_3\left(\mathbf{a}_{\alpha,\beta} \cdot \mathbf{a}_3\right), \tag{60}$$

where $\mathbf{a}_\alpha$ are the covariant base vectors of the surface, $\mathbf{a}_3$ is the unit normal, and λ_3 is the thickness stretch.

The derivatives of the internal and external virtual work with respect to the rth degree of freedom are given by

$$\delta_r\mathcal{W}_{int} = \int_{S_0} \left(\overline{\mathbf{n}} : \delta_r\boldsymbol{\varepsilon} + \overline{\mathbf{m}} : \delta_r\boldsymbol{\kappa}\right) \mathrm{d}S_0 \tag{61}$$

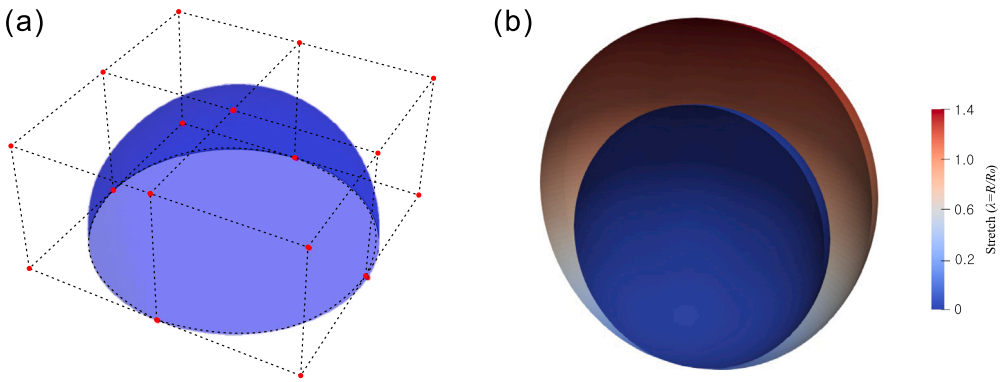

Fig. 5. Numerical simulation of the inflation of a spherical incompressible rubber balloon [64]: (a) control points (red dots), control mesh (black dashed lines), and the corresponding NURBS representation of the hemisphere (blue surface); and (b) the isogeometric finite element simulation of the inflation process. The edge boundary is subjected to a roller boundary condition, and one point at the bottom is fixed to prevent rigid-body motion. The simulation is carried out up to the snap-through limit, occurring at a circumferential stretch of $\lambda = 1.38$.

$$\delta_r \mathcal{W}_{ext} = \int_{S_0} \bar{\mathbf{f}} \cdot \delta_r \mathbf{u} \, \mathrm{d}S_0 \tag{62}$$

The global residual vector $\mathbf{R}$ of size $3n_{cp}$ is defined as

$$\mathbf{R} = \mathbf{F}_{int} - \mathbf{F}_{ext} \tag{63}$$

where $\mathbf{F}_{int}$ and $\mathbf{F}_{ext}$ are the global force vectors whose rth components are $\delta_r \mathcal{W}_{int}$ and $\delta r \mathcal{W}_{ext}$, respectively. The system is in equilibrium when the residual satisfies $\mathbf{R}_r = 0$.

For the linearization of Eq. (63), the consistent tangent stiffness matrix $\mathbf{K}$ of size $3n_{cp} \times 3n_{cp}$ is computed as

$$K_{rs} = \delta_r \delta_s \mathcal{W}_{int} - \delta_r \delta_s \mathcal{W}_{ext}, \tag{64}$$

where K_{rs} denotes the (r, s) entry of $\mathbf{K}$. The resulting linearized system is solved for the incremental displacement vector $\Delta\mathbf{u}$ using a Newton–Raphson procedure [17]:

$$\mathbf{u}_{i+1} = \mathbf{u}_i - \mathbf{K}_i^{-1} \mathbf{R}_i, \tag{65}$$

where i and $i + 1$ denote the current and next Newton iterations, respectively. The problem is solved incrementally using the Newton–Raphson method, implemented in FEniCS (version 2019.2.0) [57,58] with tIGAr [59], interfaced through PETSc/SNES nonlinear solvers [63]. The iterative process is continued until the convergence criterion is satisfied, defined by the L_2 norm of the residual vector falling below 0.1% of its initial value.

5. Numerical examples

In this section, we present two numerical examples to evaluate the accuracy, robustness, and applicability of the proposed isogeometric Kirchhoff–Love shell formulation for large deformation problems. The first example considers the inflation of a thin spherical balloon, a classical benchmark in computational solid mechanics with a known analytical solution. This test serves to validate the formulation against an established reference. The second example examines the inflation of a flat square shell, highlighting the method's capability to capture large deformations as well as the time-dependent response of viscoelastic materials.

5.1. Inflation of a thin balloon

We first consider the inflation of an incompressible hemispherical rubber balloon with radius $R_0 = 10.0$, thickness $h_0 = 0.1$, and shear modulus $\mu = 4.225 \times 10^5\,\mathrm{N/m^2}$, following the benchmark problem in [64]. As both the theoretical derivation and numerical simulation are performed in a non-dimensional setting, units for R_0 and h_0 are omitted. The hemisphere is represented exactly by a single NURBS patch; the control points, control mesh, and resulting surface are shown in Fig. 5(a). A roller boundary condition is applied along the edge, and one point at the bottom is fixed to eliminate rigid-body motion. The balloon is then pressurized internally until the onset of snap-through instability.

The material response is modeled using an incompressible hyperelastic constitutive law, while viscoelastic effects are neglected in Fig. 6 to allow direct comparison with the analytical solution. The inflation process is simulated with the proposed isogeometric Kirchhoff–Love shell formulation, where the internal pressure is linearly increased over 100 s, as shown in Fig. 6(a). The resulting internal pressure–stretch response, presented in Fig. 6(b), shows excellent agreement with the analytical prediction up to the snap-through point, which occurs at a circumferential stretch of $\lambda = 1.38$.

To further examine the viscoelastic extension of the formulation, additional simulations are performed by incorporating a non-equilibrium shear response. Fig. 7 depicts the time evolution of the non-equilibrium strain energy: Fig. 7(a) shows the effect of varying characteristic time scales, while Fig. 7(b) illustrates the influence of different ratios of elastic to viscoelastic shear moduli. In Fig. 7(a), we observe that increasing the characteristic time scale leads to a delayed peak in the non-equilibrium strain energy, accompanied by an increase in its magnitude. In Fig. 7(b), increasing the viscoelastic shear modulus results in a higher peak of non-equilibrium strain energy, while the time at which the peak occurs remains unchanged.

5.2. Inflation of a flat shell

As a second numerical example, we investigate the inflation of a flat square shell with clamped boundaries, designed to assess the ability of the formulation to capture large out-of-plane deformations in initially flat geometries. The shell has an edge length of $R_0 = 10.0$, thickness $h_0 = 0.1$, and shear modulus $\mu = 4.225 \times 10^5\,\mathrm{N/m^2}$, consistent with the parameters used in the spherical balloon example. All simulations are performed in non-dimensional form, with R_0 and h_0 omitted. The initial and deformed configurations, together with contour plots of the displacement magnitude, are shown in Fig. 8, demonstrating significant geometric nonlinearities at peak inflation.

The results are summarized in Fig. 9. Fig. 9(a) presents the normalized internal pressure–deflection curves for different shear modulus ratios. As the viscoelastic shear modulus decreases, the maximum deflection increases, reflecting a softer effective structural response. Fig. 9(b) shows the stress magnitude at the shell center as a function of the relaxation time on a logarithmic scale; larger relaxation times lead to greater peak stresses due to slower stress dissipation. These findings highlight the sensitivity of the inflation response to both the elastic–viscoelastic shear modulus ratio and the relaxation time, underscoring the robustness of the proposed formulation for strongly coupled geometric and material nonlinearities.

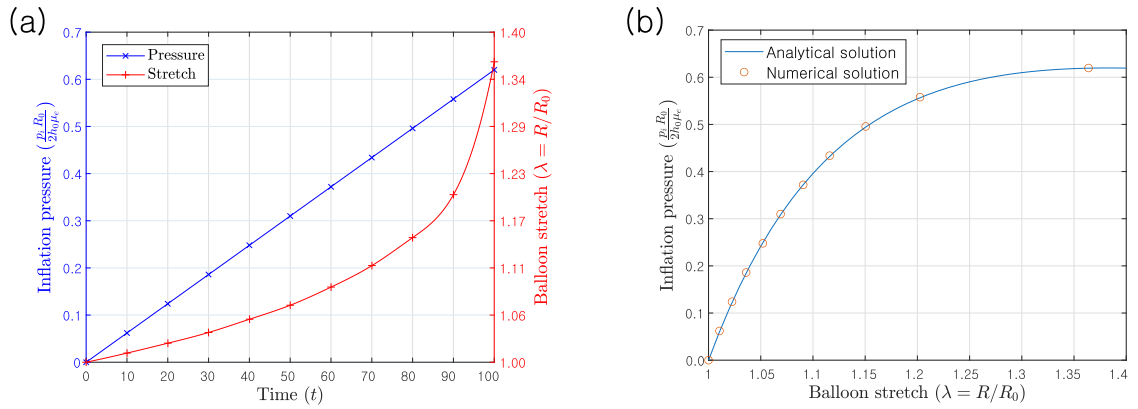

Fig. 6. Comparison between analytical and numerical results for the inflation of a spherical incompressible rubber balloon [52]: (a) time histories of internal pressure p_i (left vertical axis) and circumferential stretch λ (right vertical axis) over $t \in [0, 100]$, and (b) internal pressure p_i versus circumferential stretch λ comparing analytical and numerical solutions. All quantities are normalized for comparison. The numerical results are obtained using the proposed isogeometric Kirchhoff–Love shell formulation, neglecting viscoelastic effects to enable direct validation against the analytical solution. Excellent agreement is observed up to the snap-through limit (approximately $\lambda = 1.38$).

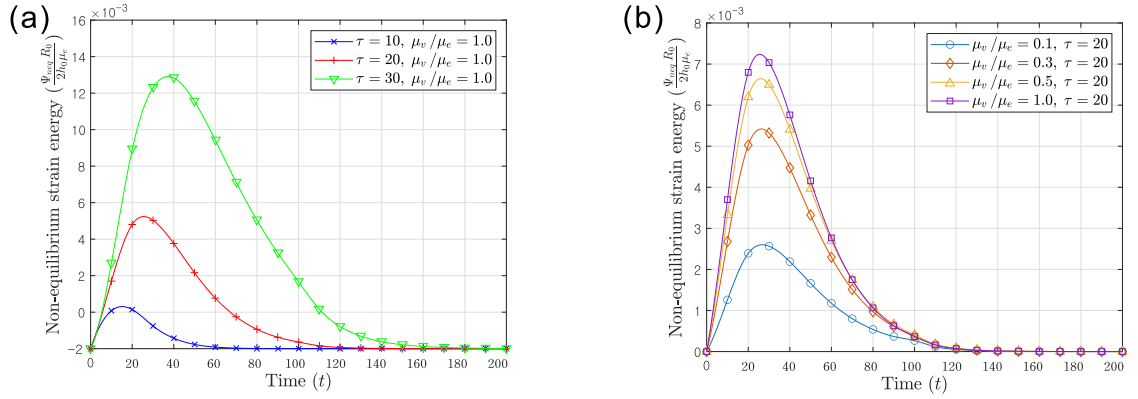

Fig. 7. Time histories from the numerical simulation of the inflation of a spherical incompressible rubber balloon: (a) non-equilibrium strain energy versus time for various characteristic time scales, and (b) non-equilibrium strain energy versus time for various ratios of shear moduli between the elastic and viscoelastic components.

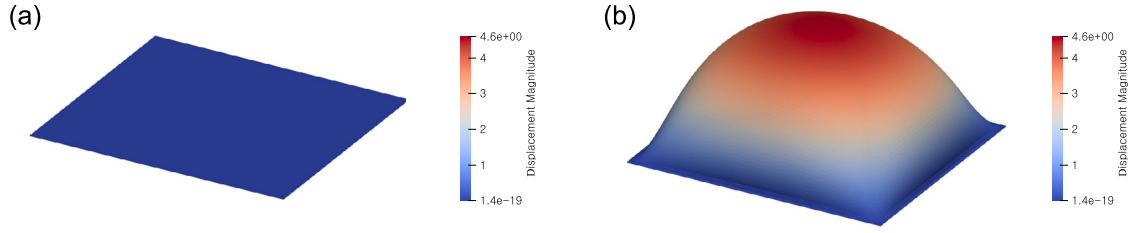

Fig. 8. Inflated square shell with contour plots of the displacement magnitude: (a) initial configuration, and (b) deformed configuration at maximum inflation.

6. Conclusion

In this study, we developed a visco-hyperelastic Kirchhoff–Love shell formulation for large-deformation, time-dependent response. The shell kinematics are formulated in a local curvilinear coordinate system on the mid-surface, decoupling the motion of the mid-surface from the rotation of the director (outward normal) vectors. We emphasize the advantages of the IGA over the standard FEA. In a standard FEA, the mid-surface is discretized by 3-node or 4-node elements; director vectors are defined at the nodes and assumed perpendicular to planar facets, which introduces inevitable geometric approximation errors. By contrast, the shell mid-surface in the IGA requires no geometric faceting and remains geometrically exact, allowing direct evaluation of C^1-dependent quantities such as curvature. This enhances geometric fidelity and provides new insights into the role of visco-hyperelasticity in large-deformation, time-dependent shell responses. For the large-deformation viscoelastic formulation, we introduced additional internal (state) variables to account for dissipation, where the time-dependent response were obtained using a backward Euler scheme. In the first numerical example, the simulation results exactly matched the analytical solution for balloon inflation, validating the implementation; and then in the second example, we investigated parameter effects on large-deformation and viscoelastic responses of a flat shell and observed that viscoelastic relaxation can produce noticeable different deformation histories compared with purely elastic behavior. Future work will extend this formulation to applications in biological materials, such as cerebral aneurysms — their inflation and instability — thereby supporting the digital health-care of clinical decision-making and patient-specific treatment.

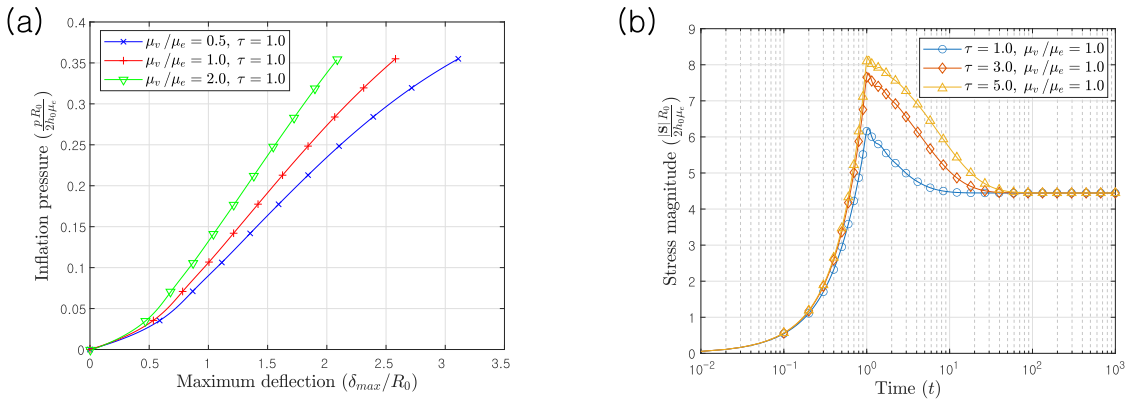

Fig. 9. Numerical results for the inflation of a square viscoelastic shell: (a) normalized internal pressure p_i versus normalized deflection for different ratios of elastic to viscoelastic shear moduli, and (b) stress magnitude at the shell center for various characteristic time scales, plotted on a logarithmic scale.

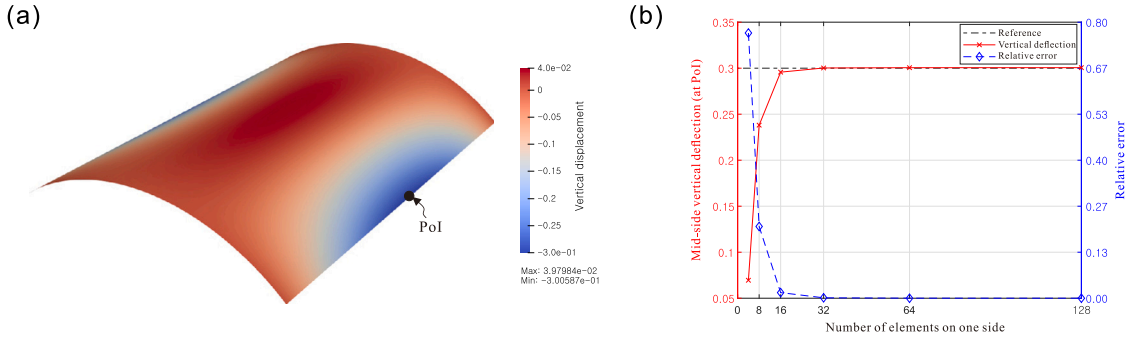

Fig. A.1. Convergence study for the benchmark problem of the Scordelis–Lo roof. (a) Representative vertical deflection field for $m = 128$, where m denotes the number of elements per side. (b) Convergence of the vertical deflection and relative error at the mid-side point of the straight edge (PoI).

CRediT authorship contribution statement

Seung-Hwan Boo: Writing – review & editing, Resources. **Hyomin Ryu:** Resources, Formal analysis, Data curation. **Seung Hwan Kim:** Writing – review & editing, Project administration, Funding acquisition. **Jaemin Kim:** Writing – review & editing, Writing – original draft, Visualization, Validation, Supervision, Software, Project administration, Methodology, Investigation, Funding acquisition, Formal analysis, Conceptualization.

Declaration of competing interest

The authors declare that they have no known competing financial interests or personal relationships that could have appeared to influence the work reported in this paper.

Acknowledgments

Jaemin Kim and **Seung Hwan Kim**: This research was funded by the 'Changwon National University - Samsung Changwon Hospital joint Collaboration Research Support Project, South Korea' in 2025. **Jaemin Kim** and **Hyomin Ryu**: Following are results of a study on the "Regional Innovation System & Education (RISE)" Project, supported by the Ministry of Education and Gyeongsangnam-do (RISE Center), Gyeongsangnam-do, funded by the Ministry of Education(MOE) and the Gyeongsangnam-do Provincial Government, Republic of Korea (2025-RISE-16-002). This study was conducted as part of the Glocal University Project, supported by the RISE (Regional Innovation System & Education) program funded by the Ministry of Education. **Seung-Hwan Boo**: This work was supported by the Ministry of Trade, Industry and Energy (MOTIE), Korea, under the Shipbuilding and Marine Engineering Technology Development Program (RS-2024-00460088).

Appendix. Convergence study for Scordelis–Lo roof

We consider the Scordelis–Lo roof problem as a classical benchmark originally proposed by [65] and later analyzed using isogeometric Kirchhoff–Love shell formulations in [16,66]. The problem consists of a cylindrical shell subjected to self-weight loading, with the quantity of interest being the vertical displacement at the mid-side of one of the straight boundaries (see Fig. A.1(a), Point of Interest (PoI)). A complete description of the problem setup can be found in [16,65,66]. Briefly, the model consists of an 80° cylindrical surface with a length $L = 50$, radius $R = 25$, and thickness $t = 0.25$. The material properties are defined by an elastic modulus $E = 4.32\times10^8$ and Poisson's ratio $\nu = 0.0$. A uniform gravity load of magnitude 90.0 is applied in the negative (downward) vertical direction.

We compare the vertical deflection v_m computed at the point of interest with the reference solution $v_{\text{ref}} = 0.3006$, using several discretizations with the number of elements $m = 4, 8, 16, 32, 64, 128$ per side, while keeping the polynomial degree fixed at $p = 2$. A representative displacement field for $m = 128$ is shown in Fig. A.1(a), and the convergence of the vertical deflection and relative error is presented in Fig. A.1(b). The numerical results exhibit excellent convergence toward the reference solution, providing the additional verification of the proposed framework.

Data availability

Data will be made available on request.

References

[1] Takashi Kuraishi, Zhaojing Xu, Kenji Takizawa, Tayfun E Tezduyar, Tsuyoshi Kakegami, Space–time isogeometric analysis of tire aerodynamics with complex tread pattern, road contact, and tire deformation, Comput. Mech. 75 (2) (2025) 575–591.

[2] Zhaowei Liu, Andrew McBride, Abhishek Ghosh, Luca Heltai, Weicheng Huang, Tiantang Yu, Paul Steinmann, Prashant Saxena, Computational instability analysis of inflated hyperelastic thin shells using subdivision surfaces, Comput. Mech. 73 (2) (2024) 257–276.

[3] San Kim, Jaemin Kim, A phase-field fracture model for 3D film–substrate systems, Int. J. Non-Linear Mech. 175 (2025) 105126.

[4] Seung-Hwan Boo, Jaemin Kim, Multiphysics modeling of surface diffusion coupled with large deformation in 3D solids, Eur. J. Mech. A Solids 113 (2025) 105713.

[5] Yuqiang Cheng, Hua Gao, Jianguo Ma, Changgeng Shuai, Stiffness analysis and structural optimization design of an air spring for ships, Sci. Rep. 14 (1) (2024) 14650.

[6] Mohan Krishna Paleti, S. Suriya Prakash, V. Narayanamurthy, A shell theory approach for the analysis of metal-FRP hybrid toroidal pressure vessels, Thin-Walled Struct. 204 (2024) 112266.

[7] Ajay Kumar, Aman Khurana, Atul Kumar Sharma, MM Joglekar, Dynamics of pneumatically coupled visco-hyperelastic dielectric elastomer actuators: theoretical modeling and experimental investigation, Eur. J. Mech. A Solids 95 (2022) 104636.

[8] Yufei Hao, Tianmiao Wang, Ziyu Ren, Zheyuan Gong, Hui Wang, Xingbang Yang, Shaoya Guan, Li Wen, Modeling and experiments of a soft robotic gripper in amphibious environments, Int. J. Adv. Robot. Syst. 14 (3) (2017) 1729881417707148.

[9] Rong Fan, Michael S. Sacks, Simulation of planar soft tissues using a structural constitutive model: finite element implementation and validation, J. Biomech. 47 (9) (2014) 2043–2054.

[10] Erik Mailand, Ece Özelçi, Jaemin Kim, Matthias Rüegg, Odysseas Chaliotis, Jon Märki, Nikolaos Bouklas, Mahmut Selman Sakar, Tissue engineering with mechanically induced solid-fluid transitions, Adv. Mater. 34 (2) (2022) 2106149.

[11] Nasser Firouzi, Rinaldo Garziera, Gerhard A Holzapfel, Timon Rabczuk, Mechanics of finite nonlinear viscoelastic growth for soft biological tissues, Thin-Walled Struct. 210 (2025) 112996.

[12] Josef Kiendl, K-U Bletzinger, Johannes Linhard, Roland Wüchner, Isogeometric shell analysis with Kirchhoff–Love elements, Comput. Methods Appl. Mech. Engrg. 198 (49–52) (2009) 3902–3914.

[13] Thomas J.R. Hughes, John A. Cottrell, Yuri Bazilevs, Isogeometric analysis: CAD, finite elements, NURBS, exact geometry and mesh refinement, Comput. Methods Appl. Mech. Engrg. 194 (39–41) (2005) 4135–4195.

[14] Thomas J.R. Hughes, The Finite Element Method: Linear Static and Dynamic Finite Element Analysis, Courier Corporation, 2012.

[15] Zhihui Zou, Thomas JR Hughes, Michael A Scott, Roger A Sauer, Eshwar J Savitha, Galerkin formulations of isogeometric shell analysis: Alleviating locking with Greville quadratures and higher-order elements, Comput. Methods Appl. Mech. Engrg. 380 (2021) 113757.

[16] Roger A. Sauer, Zhihui Zou, Thomas J.R. Hughes, A simple and efficient hybrid discretization approach to alleviate membrane locking in isogeometric thin shells, Comput. Methods Appl. Mech. Engrg. 424 (2024) 116869.

[17] Josef Kiendl, Ming-Chen Hsu, Michael CH Wu, Alessandro Reali, Isogeometric Kirchhoff–Love shell formulations for general hyperelastic materials, Comput. Methods Appl. Mech. Engrg. 291 (2015) 280–303.

[18] Peter Hansbo, Mats G. Larson, Fredrik Larsson, Tangential differential calculus and the finite element modeling of a large deformation elastic membrane problem, Comput. Mech. 56 (1) (2015) 87–95.

[19] Olgierd Cecil Zienkiewicz, Robert Leroy Taylor, The Finite Element Method for Solid and Structural Mechanics, Elsevier, 2005.

[20] Manfred Bischoff, K-U Bletzinger, WA Wall, Ekkehard Ramm, Models and finite elements for thin-walled structures, Wiley Online Library, 2004,

[21] Yongzhen Mi, Xiang Yu, Isogeometric MITC shell, Comput. Methods Appl. Mech. Engrg. 377 (2021) 113693.

[22] Les Piegl, Wayne Tiller, The NURBS Book, Springer Science & Business Media, 2012.

[23] David F. Rogers, An Introduction to NURBS: with Historical Perspective, Elsevier, 2000.

[24] Ruben Sevilla, Sonia Fernández-Méndez, Antonio Huerta, NURBS-enhanced finite element method (NEFEM), Internat. J. Numer. Methods Engrg. 76 (1) (2008) 56–83.

[25] Yu Vetyukov, Finite element modeling of Kirchhoff-Love shells as smooth material surfaces, ZAMM-J. Appl. Math. Mech./Z. Angew. Math. Mech. 94 (1–2) (2014) 150–163.

[26] Sebastian Platzer, Astrid Pechstein, Alexander Humer, Michael Krommer, Viscoelastic Kirchhoff–Love shells at finite strains: constitutive modeling and mixed low-regularity finite elements, Acta Mech. (2025) 1–20, http://dx.doi.org/10.1007/s00707-025-04255-3.

[27] Marreddy Ambati, Josef Kiendl, Laura De Lorenzis, Isogeometric Kirchhoff–Love shell formulation for elasto-plasticity, Comput. Methods Appl. Mech. Engrg. 340 (2018) 320–339.

[28] Daniel Rypl, Borek Patzák, Study of computational efficiency of numerical quadrature schemes in the isogeometric analysis, Eng. Mech. 304 (2012) 1135–1143.

[29] Daniel Rypl, Borek Patzák, Assessment of computation efficiency of numerical quadrature schemes in the isogeometric analysis, Eng. Mech. 19 (4) (2012) 249–260.

[30] Kenji Takizawa, Tayfun E Tezduyar, Yuto Otoguro, Takuya Terahara, Takashi Kuraishi, Hitoshi Hattori, Turbocharger flow computations with the space–time isogeometric analysis (ST-IGA), Comput. & Fluids 142 (2017) 15–20.

[31] Yuri Bazilevs, Kenji Takizawa, Tayfun E Tezduyar, Artem Korobenko, Takashi Kuraishi, Yuto Otoguro, Computational aerodynamics with isogeometric analysis, J. Mech. 39 (2023) 24–39.

[32] Gang Xu, Bernard Mourrain, Régis Duvigneau, André Galligo, Parameterization of computational domain in isogeometric analysis: Methods and comparison, Comput. Methods Appl. Mech. Engrg. 200 (23–24) (2011) 2021–2031.

[33] Ming-Chen Hsu, Ido Akkerman, Yuri Bazilevs, High-performance computing of wind turbine aerodynamics using isogeometric analysis, Comput. & Fluids 49 (1) (2011) 93–100.

[34] Yuri Bazilevs, L Beirao da Veiga, J Austin Cottrell, Thomas JR Hughes, Giancarlo Sangalli, Isogeometric analysis: Approximation, stability and error estimates for h-refined meshes, Math. Models Methods Appl. Sci. 16 (07) (2006) 1031–1090.

[35] Cédric Adam, Thomas JR Hughes, Salim Bouabdallah, Malek Zarroug, Habibou Maitournam, Selective and reduced numerical integrations for NURBS-based isogeometric analysis, Comput. Methods Appl. Mech. Engrg. 284 (2015) 732–761.

[36] Vibhushit Gupta, Azher Jameel, Shubham K Verma, Sanjeev Anand, Yatheshth Anand, An insight on NURBS based isogeometric analysis, its current status and involvement in mechanical applications, Arch. Comput. Methods Eng. 30 (2) (2023) 1187–1230.

[37] Vlado Lubarda, Rate-type elasticity and viscoelasticity of an erythrocyte membrane, J. Mech. Mater. Struct. 6 (1) (2011) 361–376.

[38] Fushan Li, A justification of two-dimensional nonlinear viscoelastic shells model, in: Abstract and Applied Analysis, Vol. 2012, Wiley Online Library, 2012, 287865.

[39] Erwin Hernandez, César Naranjo, Jesus Vellojin, Modelling of thin viscoelastic shell structures under Reissner–Mindlin kinematic assumption, Appl. Math. Model. 79 (2020) 180–199.

[40] Farzam Dadgar-Rad, Nasser Firouzi, Time-dependent response of incompressible membranes based on quasi-linear viscoelasticity theory, Int. J. Appl. Mech. 13 (03) (2021) 2150036.

[41] Nasser Firouzi, Krzysztof Kamil Żur, Marco Amabili, Timon Rabczuk, On the time-dependent mechanics of membranes via the nonlinear finite element method, Comput. Methods Appl. Mech. Engrg. 407 (2023) 115903.

[42] Ali Javili, Paul Steinmann, A finite element framework for continua with boundary energies. Part I: the two-dimensional case, Comput. Methods Appl. Mech. Engrg. 198 (27–29) (2009) 2198–2208.

[43] Ali Javili, Paul Steinmann, A finite element framework for continua with boundary energies. Part II: The three-dimensional case, Comput. Methods Appl. Mech. Engrg. 199 (9–12) (2010) 755–765.

[44] Berkin Dortdivanlioglu, Ali Javili, Boundary viscoelasticity theory at finite deformations and computational implementation using isogeometric analysis, Comput. Methods Appl. Mech. Engrg. 374 (2021) 113579.

[45] Jaemin Kim, Erik Mailand, Ida Ang, Mahmut Selman Sakar, Nikolaos Bouklas, A model for 3D deformation and reconstruction of contractile microtissues, Soft Matter 17 (45) (2021) 10198–10209.

[46] Jaemin Kim, Ida Ang, Francesco Ballarin, Chung-Yuen Hui, Nikolaos Bouklas, A finite element implementation of finite deformation surface and bulk poroelasticity, Comput. Mech. 73 (5) (2024) 1013–1031.

[47] Jaemin Kim, Erik Mailand, Mahmut Selman Sakar, Nikolaos Bouklas, A model for mechanosensitive cell migration in dynamically morphing soft tissues, Extrem. Mech. Lett. 58 (2023) 101926.

[48] Xiaoxiao Du, Gang Zhao, Ran Zhang, Wei Wang, Jiaming Yang, Numerical implementation for isogeometric analysis of thin-walled structures based on a Bézier extraction framework: nligaStruct, Thin-Walled Struct. 180 (2022) 109844.

[49] Yasutoshi Taniguchi, Kenji Takizawa, Yuto Otoguro, Tayfun E Tezduyar, A hyperelastic extended Kirchhoff–Love shell model with out-of-plane normal stress: I. Out-of-plane deformation, Comput. Mech. 70 (2) (2022) 247–280.

[50] Yasutoshi Taniguchi, Kenji Takizawa, Yuto Otoguro, Tayfun E Tezduyar, A hyperelastic extended Kirchhoff–Love shell model with out-of-plane normal stress: II. An isogeometric discretization method for incompressible materials, Comput. Mech. 74 (3) (2024) 561–589.

[51] Wilhelm Flügge, Tensor Analysis and Continuum Mechanics, Springer, 1972.

[52] Gerhard A. Holzapfel, Nonlinear Solid Mechanics: a Continuum Approach for Engineering, John Wiley & Sons, Inc., 2000.

[53] Morton E. Gurtin, Eliot Fried, Lallit Anand, The Mechanics and Thermodynamics of Continua, Cambridge University Press, 2010.

[54] Bernard D. Coleman, Morton E. Gurtin, Thermodynamics with internal state variables, J. Chem. Phys. 47 (2) (1967) 597–613.
[55] Christian Linder, Mykola Tkachuk, Christian Miehe, A micromechanically motivated diffusion-based transient network model and its incorporation into finite rubber viscoelasticity, J. Mech. Phys. Solids 59 (10) (2011) 2134–2156.
[56] Haiqian Yang, Thomas Henzel, Eric M. Stewart, Ming Guo, An interpenetrating-network theory of the cytoskeletal networks in living cells, J. Mech. Phys. Solids 189 (2024) 105688.
[57] Anders Logg, Kent-Andre Mardal, Garth N. Wells, Automated Solution of Differential Equations by the Finite Element Method : The Fenics Book, Springer, 2012.
[58] Martin S. Alnæs, Jan Blechta, Johan Hake, August Johansson, Benjamin Kehlet, Anders Logg, Chris Richardson, Johannes Ring, Marie E. Rognes, Garth N. Wells, The FEniCS project version 1.5, Arch. Numer. Softw. 3 (100) (2015) 9–23.
[59] David Kamensky, Yuri Bazilevs, tIGAr: Automating isogeometric analysis with FEniCS, Comput. Methods Appl. Mech. Engrg. 344 (2019) 477–498.
[60] J. Austin Cottrell, Thomas J.R. Hughes, Yuri Bazilevs, Isogeometric Analysis: Toward Integration of CAD and FEA, John Wiley & Sons, 2009.
[61] Yuri Bazilevs, Kenji Takizawa, Tayfun E. Tezduyar, Computational Fluid-Structure Interaction: Methods and Applications, John Wiley & Sons, 2013.
[62] Thang X. Duong, Farshad Roohbakhshan, Roger A. Sauer, A new rotation-free isogeometric thin shell formulation and a corresponding continuity constraint for patch boundaries, Comput. Methods Appl. Mech. Engrg. 316 (2017) 43–83.
[63] Satish Balay, Shrirang Abhyankar, Mark Adams, Jed Brown, Peter Brune, Kris Buschelman, Lisandro Dalcin, Alp Dener, Victor Eijkhout, W Gropp, et al., PETSc users manual, 2019.
[64] Gerhard A. Holzapfel, Thomas C. Gasser, Ray W. Ogden, A new constitutive framework for arterial wall mechanics and a comparative study of material models, J. Elasticity 61 (1–3) (2000) 1–48.
[65] Ted Belytschko, Henryk Stolarski, Wing Kam Liu, Nicholas Carpenter, Jame SJ Ong, Stress projection for membrane and shear locking in shell finite elements, Comput. Methods Appl. Mech. Engrg. 51 (1–3) (1985) 221–258.
[66] Masoud Behzadinasab, Mert Alaydin, Nathaniel Trask, Yuri Bazilevs, A general-purpose, inelastic, rotation-free Kirchhoff–Love shell formulation for peridynamics, Comput. Methods Appl. Mech. Engrg. 389 (2022) 114422.